

Using Light Curves to Characterize Size and Shape of Pseudo-Debris

Heather M. Rodriguez

ESCG/Jacobs Sverdrup

P.O. Box 58447, Mail code: JE104, Houston, TX 77258-8447

E-mail: heather.m.rodriguez@nasa.gov

Kira J. Abercromby

ESCG/Jacobs Sverdrup

P.O. Box 58447, Mail code: JE104, Houston, TX 77258-8447

Kandy S. Jarvis

ESCG/Hamilton Sundstrand

P.O. Box 58447, Mail code: JE104, Houston, TX 77258-8447

Edwin Barker

NASA Johnson Space Center

2101 NASA Parkway, Mail code: KX, Houston, TX 77058

Abstract

Photometric measurements were collected for a new study aimed at estimating orbital debris sizes based on object brightness. To obtain a size from optical measurements the current practice is to assume an albedo and use a normalized magnitude to calculate optical size. However, assuming a single albedo value may not be valid for all objects or orbit types and material type and orientation can mask an object's true optical cross section. This experiment used a CCD camera to record data, a 300 W Xenon Ozone Free collimated light source to simulate solar illumination, and a robotic arm with five degrees of freedom to move the piece of simulated debris through various orientations. The pseudo-debris pieces used in this experiment originate from the European Space Operations Centre's ESOC2 ground test explosion of a mock satellite. An illuminated diffuse white ping-pong ball was used as a zero-magnitude reference. Each debris piece was then moved through specific orientations and rotations to generate a light curve. This paper discusses the results of five different object-based light curves as measured through an x-rotation. Intensity measurements, from which each light curve was generated, were recorded in five degree increments from zero to 360 degrees. Comparing light curves of different shaped and sized pieces against their characteristic length establishes the start of a database from which an optical size estimation model will be derived in the future.

1. Introduction

There are two ground based methods used to acquire measurements of human-made debris currently in orbit: radar and optical telescopes. The reflected radar signal provides a measure of the radar cross section (RCS), which can be converted to size, but it is unclear if radar and optical measurements yield the same size estimates. Objects observed in the optical regime can appear bright or dark due to material type and orientation rather than being a true assessment of its optical cross section (OCS). Presently, the albedo used for optical size conversions is 0.2 for objects in geosynchronous Earth orbits (GEO) [1] and 0.1 in low Earth orbits (LEO) [2]. This study is the beginning step towards the ultimate goal of creating an optical size estimation model that is not dependent on a generic albedo assumption. An optical size estimation model is needed to provide a more statistically accurate albedo distribution for orbital debris. Ideally, RCS-derived sizes and optically-derived sizes will be comparable. The research and analysis within this project will also attempt to understand the complex light curves seen in actual observations of satellites and debris.[3], (see section 5.3).

2. Laboratory Set-up

This photometric study takes brightness measurements of orbital debris of various shapes but approximately same characteristic length at five degree phase angle steps. Future measurements will acquire sets of data with different phase angles. Phase angle is defined here as the angle between the observer, the object, and the solar illuminator.

Each piece is rotated 360 degrees in five degree increments along the x-axis to generate a light curve. Future robotic maneuvers will include more complex rotations and rotations along different axes. The debris pieces used originate from a ground test explosion of a mock upper stage rocket body from European Space Operations Centre's ESOC2 test [4]. Each debris piece is composed of an unpainted aluminum alloy and the mass is limited to 113 grams or less because of robot hardware constraints. A white ping-pong ball is used as a zero magnitude diffuse reference.

To simulate solar illumination the experiment uses a 3.3 cm collimated beam from a 300 W Xenon Ozone Free light source with a spectral range of 200 to 2500 nanometers. The beam has a 0.5 degree divergence, which is equivalent to the size of the Sun as seen from Earth. The CCD camera used to digitally record all images is an SBIG 512 x 512 ST8X MEI. The Lynx 6 robotic arm, seen in Fig. 1, is used to rotate objects through five degrees of freedom (base rotation, shoulder, elbow, wrist, and wrist rotation) in addition to having a functional gripper. The height of the robot arm when in stow position is 14 cm and reaches up to 45.7 cm when fully extended. The arm reach forward is 36.8 cm and the gripper has a full opening of 5.1 cm.

The current set-up uses two apertures (the first approximately 7.5 cm and the second 3.3 cm in diameter) in the light path to help reduce off-axis scattered light from the incoming beam. Attached to the second aperture are two neutral density filters (ND2 and ND4) to reduce the intensity level of the light at the debris piece.

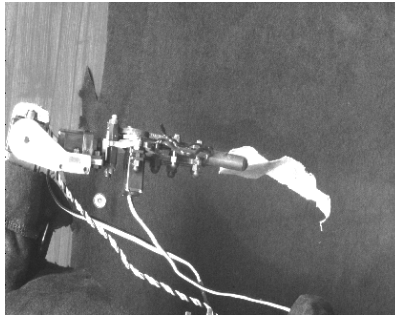


Fig. 1: Picture of robot arm holding a piece of debris from ESOC2 test.

3. Data Measurements

A set of 30 images were taken of a flat white board to be used as flat image reference for a two second exposure. The background intensity levels are relatively high (~200 counts) due to the bright light source. If the right exposure time is not chosen, some of the shadowed areas of the piece have essentially the same values as the background and are erroneously set to zero (See Section 4) producing a misleading projected area. An exposure time of two seconds was chosen for this data set after several tests were run to determine which exposure time provided the most accurately calculated area (number of non-zero pixels) for the pieces. The CCD software manual [5] recommends that the peak brightness level of each individual flat field be one-half to two-thirds of the CCD saturation levels. The 30 flat images are then stacked together so the maximum signal to noise is within a 0.5% error, only using the images that are within this percent error (approximately 14 flats are used for a two second exposure). The shorter the time of exposure the more flat images needed to reach a maximum of 0.5% variance. The final set of flat images are then averaged and applied to the final processed object image to remove any hot pixels or pixel-to-pixel sensitivity variations.

The robot held the diffuse reference (white ball) and five images were collected, summed and averaged to create an average zero magnitude reference. All data collected for this paper are reported in terms of relative magnitude, using the zero magnitude as a baseline. Data were collected on five pieces from the ESOC2 debris collection. The robotic arm was programmed to rotate each object 180 degrees in five degree increments. Once the program was finished the object was rotated manually 180 degrees. The robot program was then run in reverse to obtain a full 360 degrees rotation. Manual repositioning (i.e. manual rotation of the piece) may impact repeatability, as seen in the light curves to follow. Future programming will include a lazy susan device to remove human interaction at the 180 degree transition. A dark image was taken before each illuminated image to compensate for any thermal effects. The CCD must be kept at negative five degrees Celsius to eliminate most of the dark current and the dark frame helps remove any leftover thermal noise. The final image is produced using the following formula [6]:

$$\text{Final Processed Image} = (\text{Raw} - \text{Dark})/\text{Flat}$$

4. Analyzing Data

An internally developed MATLAB® script is used to determine the intensities of the final processed images at various orientations as well as to remove the background signal. Prior to the following methodology for removing background pixels, the initial process did not account for pixels on the object that may have the same intensity values as the background; therefore part of the object (especially on the edges) were being removed with background pixels. The current method to remove the background involves a rectangle encompassing the most illuminated area chosen manually such that it has no contamination from the debris piece or its shadow. The mean, standard deviation, minimum, and maximum of the background are calculated for this rectangle. The background level is determined by adding 3 times the standard deviation to the mean level of the background. Another rectangle is defined manually that includes the debris piece created by a cropped image of the original. Using the cropped image of the object, all pixels that are less than the determined background level are set to zero. The image is then converted to a binary image of all ones (object) and zeros (background). A 3 x 3 matrix of pixels is applied through morphology operators to the entire image to fill in gaps within the object boundaries and remove remaining pixels outside the object boundaries. This method has proved to be the best for removing background pixels with the least object pixels included to date.

Once this process is completed, a new image is created by multiplying the image of the cropped original object by the binary image to retain the original intensity values in the image. The new image is converted into a scaled color map for optimal viewing. The relative absolute magnitude (M) of each object is calculated using the following formula [7]:

$$M(\text{object}) - M(\text{white ball}) = -2.5 * \log_{10} [\text{intensity}(\text{object}) / \text{intensity}(\text{white ball})]$$

The most appropriate exposure time was determined by running several tests against five different objects of the same material type, but of different shape and size. The number of “on-pixels” is defined as the number of pixels that were counted as the object and not part of the background. The more “on-pixels” counted per object the more surface area that is viewable. This study used a two second exposure and a 360 degree rotation for all objects, but future results may use a shape and size dependant time exposure.

5. Results

5.1 Data Definitions

The five objects used for the study are named by their final placement after the explosion; alpha letters describe the circular section of the mock satellite foam catch and the numbers describe the placement down the length of the catch. The characteristic length, L_c , of each piece was measured and determined by the following equation:

$$L_c = \left(\frac{X + Y + Z}{3} \right),$$

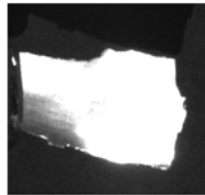
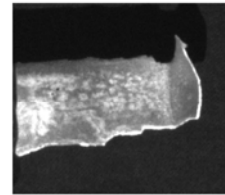
where X is deemed the longest dimension of an object, Y is the longest dimension perpendicular to X, and Z is the longest dimension perpendicular to both (i.e., the height of the object). For this experiment the grippers of the robot were blocking parts of the object from being imaged so a black rubber band was placed around each debris piece as a means to determining the “viewable L_c ” based on what is recorded on the CCD. Table 1 gives the shape, the viewable size dimensions for each piece used in this paper and the average number of pixels over all rotations for the object.

Table 1: Characteristic Length of pieces

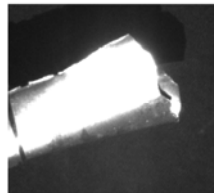
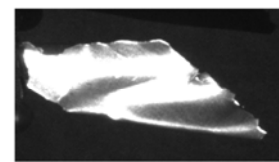
Object	Shape	X (cm)	Y (cm)	Z (cm)	Viewable L_c (cm)	Average # of Pixels
D4	Flat plate	5.7	3.6	0.7	3.33	2.72E+04
Q1	Bent Flat plate	5	2.8	1.4	3.07	2.00E+04
C2	Curled Plate	4.8	3.1	2.4	3.43	2.66E+04
P5	Folded plate	7.1	2.6	1.9	3.87	2.15E+04
E2	Torn flat plate	6.7	3.4	1.5	3.87	2.45E+04

The shape description for each object is dependant on the visual characteristics as determined in this study, regardless of the surface contamination (roughness, scratches, foam particles) of the object. An object that is 75% to 100% relatively flat is described as a flat plate. When describing a flat surface in this paper, the surface is flat relative to this set of debris and should not be compared to other possible space debris, such as solar panels. A flat plate that is bent 45 degrees to 90 degrees perpendicular to the flat part of the plate is a bent plate. A torn plate looks similar to a flat plate, but has areas that have been torn perpendicular to the flat plate orientation. If an object has approximately half of its area folded onto itself with area-to-area contact, this object is described as a folded plate. Similar to the folded plate, an object that is folded, but not in contact with any other areas is considered curled. The shape definitions used in this study are just initial categorizations that may change with different materials and more diverse collections.

Object D4, shown in Fig. 2, has the second smallest characteristic length in the sample set but it has the most measured “on-pixels” due to its flat shape. Fig. 3 shows object Q1, a bent plate with the smallest characteristic length of the sample set and as expected, the least number of “on-pixels.”

**Fig. 2. D4, flat plate, initial position****Fig. 3. Q1, bent plate, initial position**

Object C2, seen in Fig. 4, is a curled flat plate, giving it a “c” shape. Object P5, one of the objects with the largest characteristic length of the sample set, is a folded plate and is depicted in Fig. 5.

**Fig. 4. C2, curled plate, initial position****Fig. 5. P5, folded plate, initial position**

The last piece, object E2 in Fig. 6, is a ripped/torn flat piece. Object E2 is also one of the largest pieces compared to the rest of the group, but does not produce the largest amount of “on-pixels.” The three-dimensional shape of an object directly affects projected area of an object through digital approximations. This small study shows the correlation between the number of illuminated pixels and size determination is not one to one for these objects of similar size. More discussion on the number of “on-pixels” shown compared to the shape of an object to follow in section 5.4.

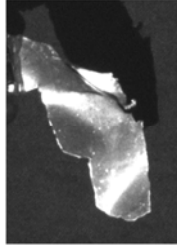


Fig. 6. E2, torn plate, initial position

5.2 Light Curves

The light curves generated for this study are presented in two ways: Intensity versus Rotation and Relative Magnitude versus Rotation. The Intensity versus Rotation shows an object's true intensity. The Relative Magnitude plot gives more insight into the light curve structure and is relative to the white ball zero magnitude reference. Both plots show two light curves that relate to the total image and the image after the background is removed. The total image is the cropped image that includes background values. The first light curve plotted, in blue circles, is from the total image. The second light curve, marked with red 'x' points, shows the plot of the image once the background is set to zero. The intensity units on the following figures are standard Analog to Digital Units (ADU). The CCD used in this experiment has a 16 bit Analog to Digital (A/D) converter with an A/D Gain of 2.3 electrons per ADU [5].

The flat piece (D4) and bent piece (Q1) of debris (Fig. 7 and Fig. 8, respectively) have similar intensity light curves; however, the peak brightness is seen at different rotation angles due to the orientation of each piece at zero degree rotation and the shape difference. Both light curves remain featureless throughout the rotation except for the two maximums around 170 degrees and 350 degrees. Object D4 has a maximum initially, which is a continuation of the 360 degree maximum. Each piece must be held differently due to its shape and the strength of the robot grippers. Future plans include orientating the piece with the minimum surface area viewable to the observer so that the maximums are continuous. The manual rotation at 180 degrees is easily seen in object Q1, where the light curve drops from approximately 3.5×10^8 ADU to approximately 0.5×10^8 ADU. This problem will be addressed in future tests with a specifically designed lazy susan device to remove human interaction with the object for the transition at 180 degrees.

The magnitude light curves in Fig. 7 and Fig. 8 show more detail in the minimum and maximum values. As expected for the two flat plates, there are two minimums and two maximums, although the bent plate light curve has structure compared to the relatively featureless light curve of the flat plate (Fig. 7).

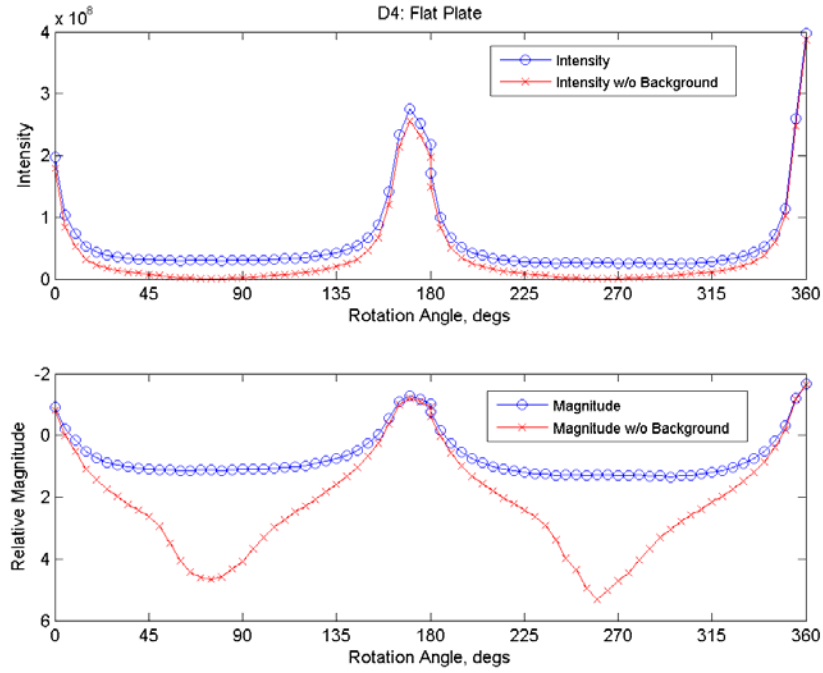


Fig. 7. D4, flat plate, Intensity and Magnitude Plots.
Note: 0 and 360 degree discrepancy is due to robot limitations.

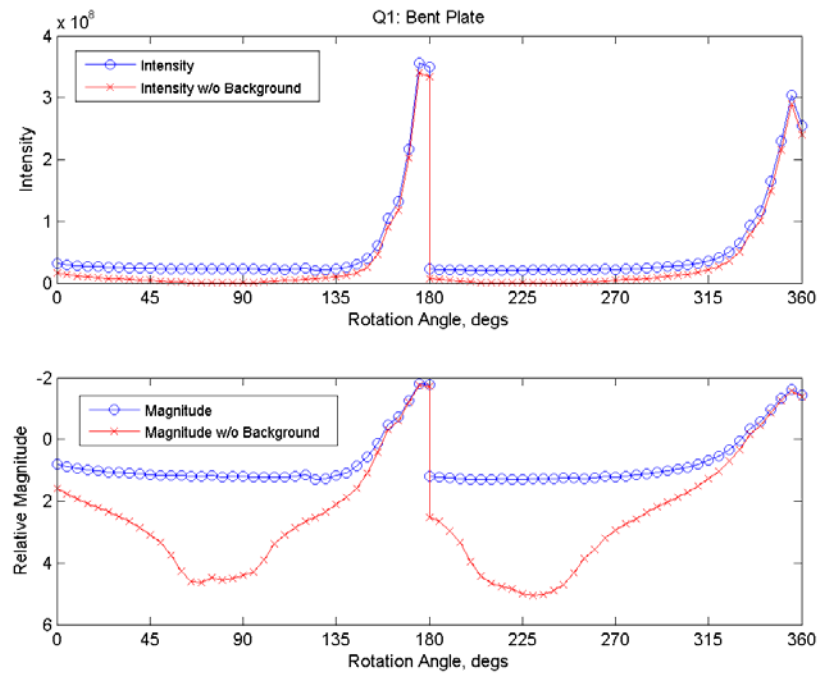


Fig. 8. Q1, bent plate, Intensity and Magnitude Plots.
Note: 0 and 360 degree discrepancy is due to robot limitations;
180 degree shift is due to manual re-orientation.

The folded and curled pieces, C2 and P5, have similar characteristics in their intensity light curves as seen in Fig. 9 and Fig. 10. Compared to the light curves of flat piece D4 and bent piece Q1, the light curves of C2 and P5 have

structure. The structure in the light curve of C2 around 265 degrees is due to the multiple light reflections from within the curved shape of the object. A similar but more oscillatory structure is visible in object P5 between 35 and 150 degrees, and is due to the multiple reflections from the torn structure of the object. The folded area of object P5 is too tight to view internal reflections like those seen in object C2's light curves. Another difference in the folded and curled plate pieces as compared to the flat plates is that the intensity curves with and without the background removed are less similar to one another. This characteristic comes mostly from shadowing on top of the object from its own curves or folds. The intensity in the shadowed areas is equal to that of the background; therefore these areas of low intensity are removed in the background removal process.

A structure that originates from processing is the shift in both light curves between 70 – 75 degrees. Depending on the complexity and shape of a piece, it is sometimes necessary to resize the cropping rectangle around the object during different rotation points to keep the object within the viewing limits. This is also noted in object E2 (Fig. 11). The resized cropping is evident when the total image light curve shows a discontinuity. Note that the background removed light curve shows no corresponding feature. The fact that the background removed light curve is not affected by user cropping shows that the background removal technique is working.

The magnitude light curves of object C2 and P5 in Fig. 9 and Fig. 10 show more structure than the previous two objects and do not present a clear double maximum and minimum as in Fig. 7 and Fig. 8. Object C2 has a minimum present at 70 degrees and structure between 200-350 degrees. Object P5 shows one clear minimum at 260 degrees.

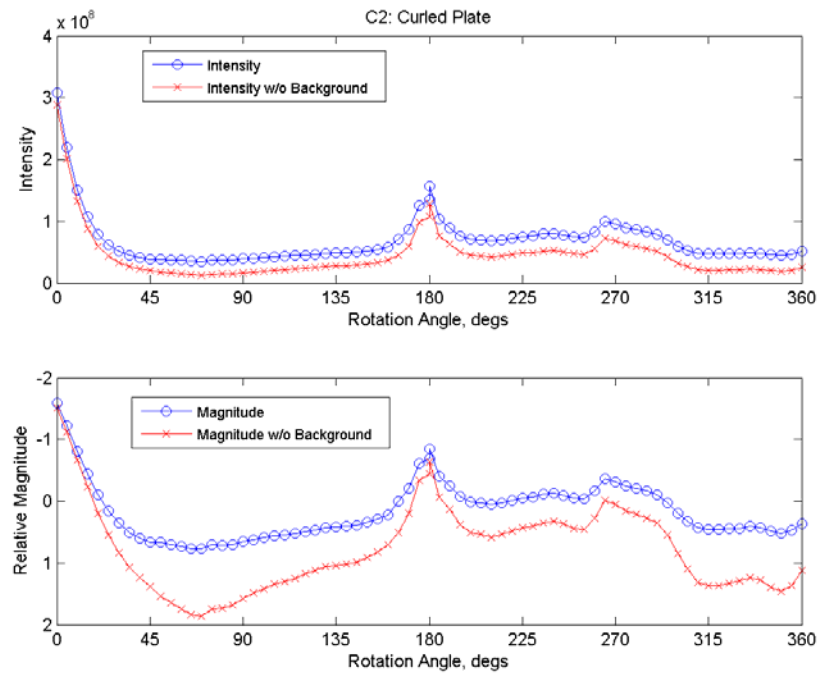


Fig. 9. C2, curled plate, Intensity and Magnitude Plots.
Note: 0 and 360 degree discrepancy is due to robot limitations;
180 degree shift is due to manual re-orientation

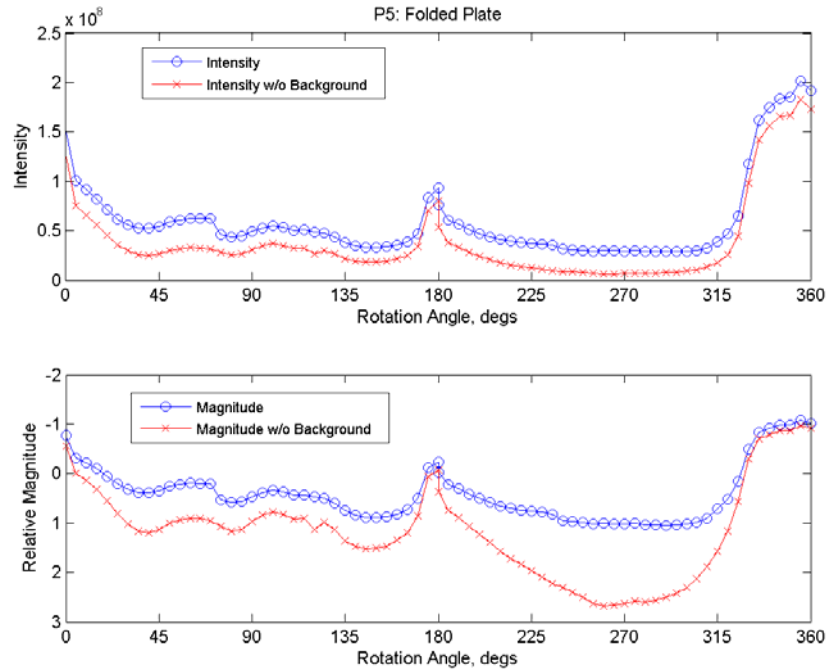


Fig. 10. P5, folded plate, Intensity and Magnitude Plots.
Note: 0 and 360 degree discrepancy is due to robot limitations;
180 degree shift is due to manual re-orientation.

The torn piece of debris, E2, has physical characteristics similar to objects C2 and P5; this similarity is not reflected in its light curve (See Fig. 11). The object is mostly flat but has been torn perpendicular to the flat area, creating similar shadowing as a folded/curved piece of debris might have. The shadowing creates the discrepancy between the total image light curve and the background removed light curve. The structure property due to user cropping is visible in Fig. 11 at the 85-120 degree and the 260-300 degree rotation points. The intensity is one magnitude fainter than all the other objects in this study and is attributed to the physical shape characteristics of this object that create more shadowing on itself than do the other curved or folded objects.

The magnitude light curve of the torn plate, E2, seen in Fig. 11 shows similarities with that of the flat plate in Fig. 7 and the bent plate in Fig. 8. Two maximums and two minimums are present and also follow a featureless light curve.

A similar characteristic among object E2 (torn) and the objects C2 (curled) and P5 (folded) is the shift between the image intensity curve and the background removed curve. This is due to shadowing on the object and pixels being removed during the background removal process. The maximum peak and secondary peak difference for all the objects is also noteworthy. The maximums for object C2, P5, and D4 all have an intensity difference of approximately 1×10^8 ADU for the intensity with background removed. One would expect the flat piece D4 to have closer values between the two maximum intensity peaks, but the manual transition at 180 degrees may incorporate a slight angle change relative to the CCD that would affect the maximum values. Object Q1 shows a smaller difference in the maximums with a value of approximately 5×10^7 ADU. The last object, E2, had the smallest variation in maximum peaks with a difference of 7×10^6 ADU. The maximum peak difference values also depend on the magnitude in the intensity data points; therefore object E2 seems to have the closest maximums, but it also had an intensity that was a magnitude lower than the other four pieces.

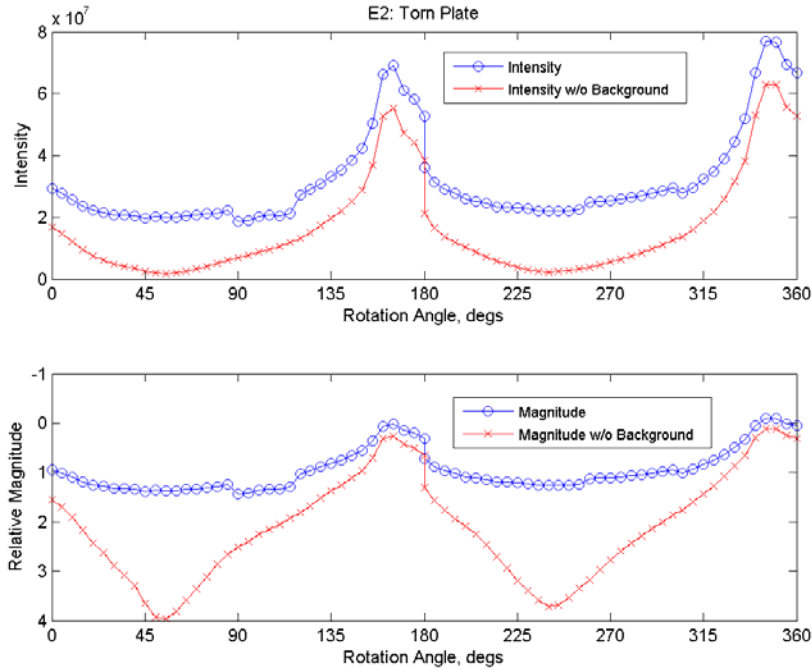


Fig. 11. E2, torn plate, Intensity and Magnitude Plots.
Note: 0 and 360 degree discrepancy is due to robot limitations;
180 degree shift is due to manual re-orientation

5.3 Shape and Orientation

There are observational studies already underway with the shape and orientation of objects, but they involve satellites and asteroids. One an example is shown in Fig. 12 [3] of a stabilized satellite (box shape with antenna) with the varying magnitude for the object over five minutes. The maximums in Fig. 12 represent glints from the antenna, similar to light curves seen over one rotation of the debris piece in this study. Future plans to decrease the five degree increment to one degree increments for the robotic arm should show more detail to the debris glints as seen in the satellite light curve.

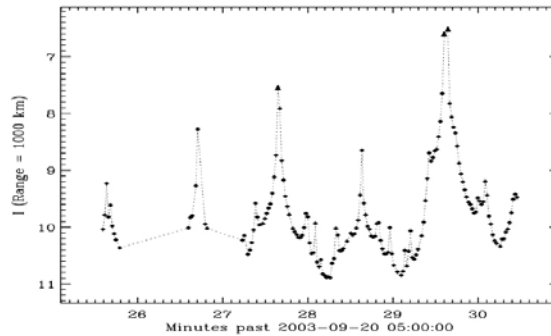


Fig. 12. Photometric Light Curve for a sample satellite.

5.4 On-Pixels

The “on-pixel” values are a little more difficult to utilize towards shape characterization and size estimation at this point. Future work with more objects will eventually lead to correlating “on-pixels” to the characteristic length of each object. Also a shape characterization against the number of “on-pixels” should show a trend. Currently, the data set used in this study is too small of a sampling to make a definitive correlation.

The flat objects would be expected to have the largest number of “on-pixels”, as was seen for D4, and lowest numbers would originate from non-flat plates like Q1 and P5. The curled plate was not expected to have such a high

number of “on-pixels”, but the internal reflections within the curved structure could increase the amount of light being reflected substantially. Also, the curled plate light curve looks similar to the flat plate light curve until the curled plate surface is viewable to the observer. Object E2, torn plate, was also surprising in respect to the amount of light being reflected, since it showed a significant shift in the intensity curve between the total image curve and the background removed curve due to the object shadowing from its own structure.

6. Conclusions

Five debris objects of the same relative size but differing shapes are confirmed to have varying light curves based on their shape complexity. Regardless of shape (within the shape types of the sample set), two maximums will occur in the intensity plot. Because the shapes are not symmetric a difference between the intensity maximum peaks is seen. The shadowing from the surface structure on the folded, curled, and torn plates is visible through the shift in light curves when the background was removed from the total image. The background removal technique proved to be effective as evidenced by the unaffected background removed light curve when the user re-cropped the object rectangle. It was speculated that the folded and curled plates would have similar light curves. Although they both showed structure, it was due to different surface areas of each piece and not just the folded/curled area. The curled piece showed structure due to reflections within the curled area, but the folded piece displayed structure due to torn areas of the piece and not due to the folded area. Therefore, these two pieces were not as similar in shape characterization as hoped for. Any attempts to correlate objects with shape categories will require many more light curve samples.

It was shown that shape and relative size can affect the number of “on-pixels” significantly. The flat plate had the most average number of “on-pixels” and the bent plate had the smallest number of “on-pixels.” Due to the small sampling in this study, a definite correlation between shape and the average number of pixels could not be concluded. A size correlation to the average number of pixels also proved to not be evident and needs more investigation. An initial starting position should be adjusted so the full maximums were not at the manual transition point of 180 degrees. This study showed there is a need to remove user interaction; therefore a lazy susan device is proposed to remove the shift at the 180 degree rotation point. More analysis is underway to understand the intensity and magnitude light curves.

This study has shown that there are some similarities between the light curves of debris pieces used and sample satellite mentioned earlier. Attempts to understand the complex light curves seen in actual observations of satellites and debris will be pursued through more analysis of light curves and larger samplings.

This experiment has never been attempted before in respect to orbital debris and optical modeling; therefore some areas are unknown and involve a trial and error process. This limited data set was used as the initial development of the measurement techniques needed for future progress. As time and studies continue, new operational information about improving this study arises. Future plans will include different phase angles, color filters, and expanding the sample set in terms of sizes and shapes. The current study is just beginning, but using light curves to help determine orbital debris shape and sizes appears promising. The ultimate goal is to develop an optical size estimation model comparable with the radar size estimation model.

7. References

1. Talent, D.L, A. Potter, and K. Henize, “A Search for Debris in GEO”, *Proceedings of the Second European Conference on Space Debris*, Darmstadt, Germany, 1997.
2. Henize, K. and J. Stanley, “Optical Observations of Space Debris”, *AIAA*, Baltimore, MD., April, pp.99-1340, 1990.
3. Sydney, P, J. Africano, and T. Kelecy, “High Precision Satellite Astrometry and Photometry”, 2004 AMOS Technical Conference Proceedings, Kihei, Maui, HI, pp 211-221, 2004.
4. Fucke, W. and H. Sdunnus, “Population Model of Small Size Space Debris” *ESPC Contract No. 9266/90/D/MD*, Battelle-Institut, BF-R 67.698-5, April 1993.
5. SBIG Astronomical Instruments, Users Guide: CCDops Version 5, November 2003.
6. Howell, S., “Handbook of CCD Astronomy”, Cambridge University Press, 2000.
7. Carroll, B. and D. Ostlie, *Modern Astrophysics*, Addison-Wesley Publishing Company, INC., 1996.